Photoacoustics 38 (2024) 100634

Contents lists available at ScienceDirect

Photoacoustics

journal homepage: www.elsevier.com/locate/pacs

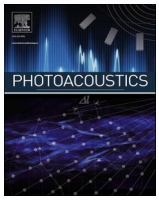

High-sensitivity trace gas detection based on differential Helmholtz photoacoustic cell with dense spot pattern

Chu Zhang, Ying He, Shunda Qiao, Yahui Liu, Yufei Ma *

National Key Laboratory of Laser Spatial Information, Harbin Institute of Technology, Harbin 150001, China

ARTICLE INFO

Keywords:
DHPAC
Dense spot pattern
Photoacoustic spectroscopy
C_2H_2 detection
MDL

ABSTRACT

A high-sensitivity photoacoustic spectroscopy (PAS) sensor based on differential Helmholtz photoacoustic cell (DHPAC) with dense spot pattern is reported in this paper for the first time. A multi-pass cell based on two concave mirrors was designed to achieve a dense spot pattern, which realized 212 times excitation of incident laser. A finite element analysis was utilized to simulate the sound field distribution and frequency response of the designed DHPAC. An erbium-doped fiber amplifier (EDFA) was employed to amplify the output optical power of the laser to achieve strong excitation. In order to assess the designed sensor's performance, an acetylene (C_2H_2) detection system was established using a near infrared diode laser with a central wavelength 1530.3 nm. According to experimental results, the differential characteristics of DHPAC was verified. Compared to the sensor without dense spot pattern, the photoacoustic signal with dense spot pattern had a 44.73 times improvement. The minimum detection limit (MDL) of the designed C_2H_2-PAS sensor can be improved to 5 ppb when the average time of the sensor system is 200 s.

1. Introduction

Trace gas detection technology is extensively applied in the fields such as atmospheric environmental monitoring, industrial process control, and medical noninvasive diagnosis [1–9]. Due to the advantages of short response time, high sensitivity and selectivity, non-invasive and real-time detection, laser absorption spectroscopy-based technology has become a research hotspot in trace gas detection [10–20]. Among these absorption spectroscopy technologies, photoacoustic spectroscopy (PAS), as a zero-background method, has the merits of simple structure, low cost and no wavelength dependence [21–27].

Resonant photoacoustic cell, as the place where the photoacoustic effect is generated, can achieve resonant amplification for photoacoustic signals [28–30]. According to the different design principles, the resonant photoacoustic cell can be categorized into several distinct types: 1) H-type photoacoustic cell; 2) T-type photoacoustic cell; 3) spherical photoacoustic cell; 4) Helmholtz photoacoustic cell [31–38]. For low acoustic and electric noise characteristics and high sensitivity, differential photoacoustic cells have emerged, which can not only double the amplitude of the photoacoustic signal, but also effectively eliminate incoherent noise caused by airflow noise and external noise [39–42].

In addition, a traditional differential photoacoustic cell mainly consists of two completely independent resonant tubes [43–46]. If the modulated incident light completely passes through one of the resonators, it is called a single excitation. More recently, in order to increase the excitation times of incident laser, the concept of introducing multi-pass cells into photoacoustic cells has attracted widespread attention for PAS gas sensor [47–50]. In 2022, Zhao et al. presented a PAS gas sensor, in which a Herriott-type multi-pass cell was placed inside the differential H-type photoacoustic cell to realize 30 times excitation of incident laser [51]. Compared with single excitation, current research on multi-pass differential photoacoustic cells has increased excitation times of incident light to a certain extent. However, there are still problems such as the inadequate excitation times of incident light and the detection performance of the system still needs to be improved.

In this paper, a high-sensitivity PAS gas sensor based on differential Helmholtz photoacoustic cell (DHPAC) with dense spot pattern is demonstrated, which realize 212 times excitation of incident laser. Finite element analysis was utilized to determine the sound field distribution and frequency response of the designed DHPAC. A multi-pass cell based on two concave mirrors was designed to achieve a dense spot pattern. In order to assess the designed sensor's performance, acetylene (C_2H_2) was chosen as the target analyte.

* Corresponding author.
E-mail address: mayufei@hit.edu.cn (Y. Ma).

https://doi.org/10.1016/j.pacs.2024.100634
Received 14 May 2024; Received in revised form 2 July 2024; Accepted 7 July 2024
Available online 9 July 2024

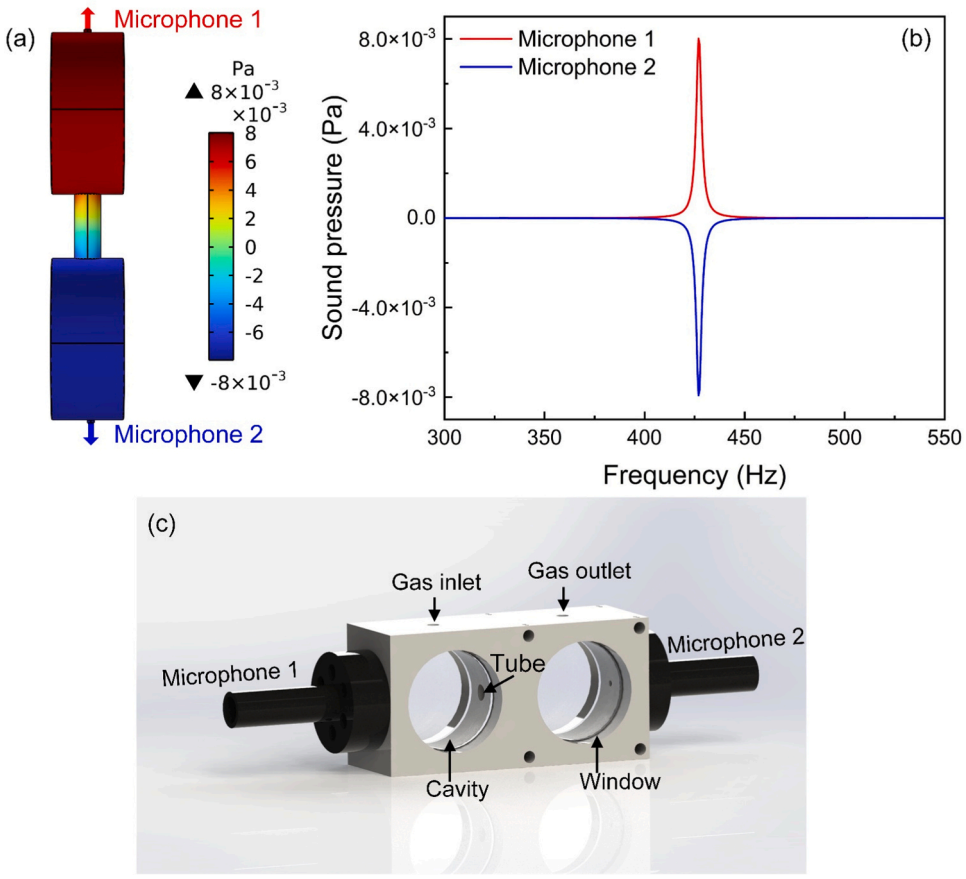

Fig. 1. (a) Sound field distribution of DHPAC. (b) Frequency response of DHPAC. (c) 3D structure of DHPAC.

2. Design of the DHPAC with dense spot pattern

2.1. Design of the DHPAC

Compared with other types of photoacoustic cells, the excitation cavity of Helmholtz photoacoustic cell has a large volume and is easier to combine with a multi-pass cell, which can achieve more excitation times of incident light. Meanwhile, the differential mode can double enhance the photoacoustic signal and suppress incoherent noise. Therefore, a DHPAC is designed in this experiments to achieve the combination of a photoacoustic cell and a multi-pass cell. The length of designed DHPAC cavity was set as 22 mm. The length of designed DHPAC connecting tube was set as 20 mm. The radius of cavity and connecting tube were set to 25 mm and 4 mm, respectively. The diameters of the microphone hole and the gas path inlet and outlet apertures were 3 mm and 4 mm, respectively.

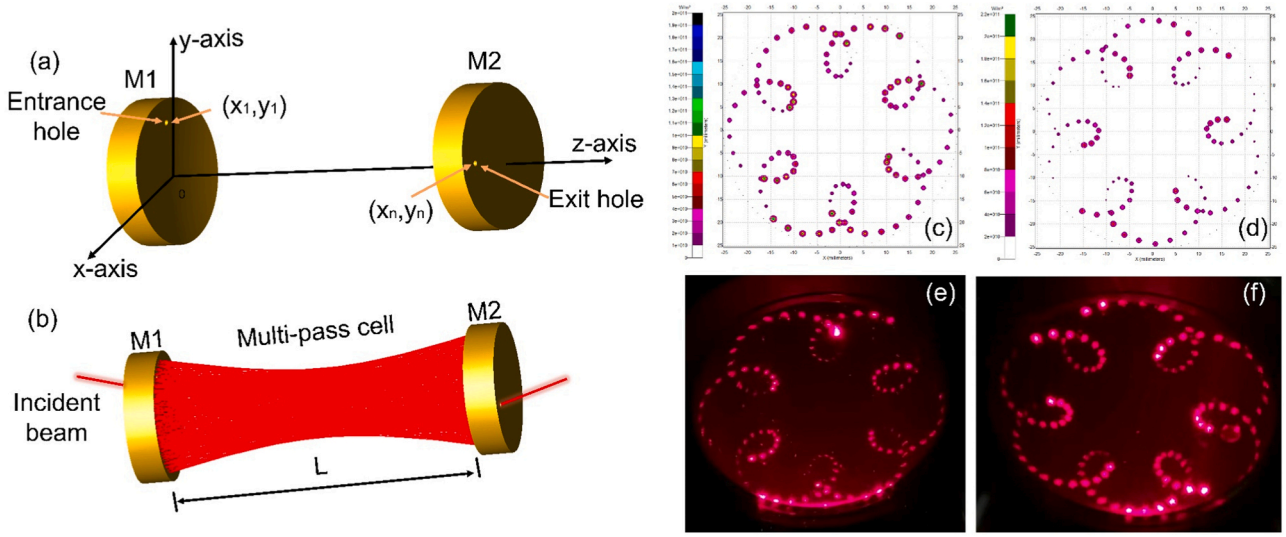

Fig. 2. (a) Schematic diagram of multi-pass cell. (b) The optical path of multi-pass cell. (c) Simulation results of incident mirror. (d) Simulation results of exit mirror. (e) Actual light spot distribution of incident mirror. (f) Actual light spot distribution of exit mirror.

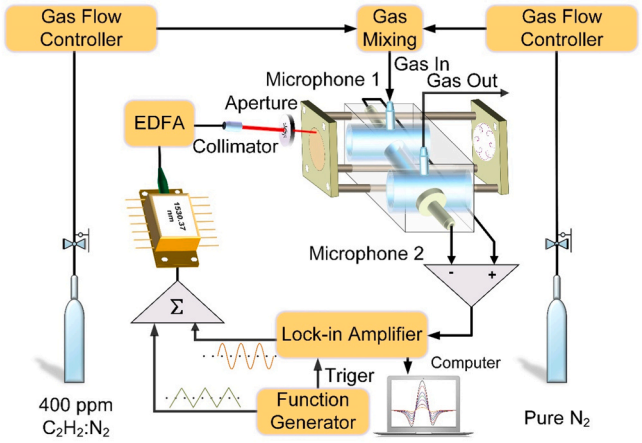

Fig. 3. Schematic diagram of the C_2H_2-PAS sensor based on DHPAC with dense spot pattern.

In order to study the acoustic characteristics of designed DHPAC, a finite element analysis model was established to simulate the acoustic field distribution and frequency response based on thermoviscous acoustic module. To obtain accurate results, viscous and thermal surface loss were considered. The sound field distribution of DHPAC is depicted in Fig. 1(a). Furthermore, two microphones are installed at both ends of the two cavities to obtain the strongest photoacoustic signal. Fig. 1(b) simulate and plot the frequency response of DHPAC. The resonant frequency of DHPAC can be obtained as 427 Hz. The 3D structure of the designed DHPAC is shown in Fig. 1(c).

2.2. Design of the multi-pass cell

For achieve more excitation times of incident light, a multi-pass cell based on two identical concave mirrors was designed to achieve a dense spot pattern. In the paraxial analysis of a multi-pass cell based on two concave mirrors, the ABCD matrix of one pass count is described in Eq. (1), which consists of a standard transmission matrix and a standard reflection matrix [52].

$$\begin{bmatrix} A & B \\ C & D \end{bmatrix} = \begin{bmatrix} 1 & 0 \\ -2/R & 1 \end{bmatrix} \cdot \begin{bmatrix} 1 & D \\ 0 & 1 \end{bmatrix} \tag{1}$$

The operators S and L are introduced to eliminate the paraxial approximation. The modified ABCD matrix can be obtained [52]:

$$\begin{bmatrix} A & B \\ C & D \end{bmatrix} = \begin{bmatrix} 1 & 0 \\ L & 1 \end{bmatrix} \cdot \begin{bmatrix} 1 & d_n S \\ 0 & 1 \end{bmatrix} \tag{2}$$

Therefore, the ray parameters after the nth pass count are determined using the updated ABCD matrix [52]:

$$\begin{aligned} x_n &= x_{n-1} + d_n \cdot \sin x'_{n-1}; x'_n = -2 \cdot \arcsin x_n / R + x'_{n-1} \\ y_n &= y_{n-1} + d_n \cdot \sin y'_{n-1}; y'_n = -2 \cdot \arcsin y_n / R + y'_{n-1} \end{aligned} \tag{3}$$

The diameter and curvature radius of the concave mirror were set to 50.8 mm and 100 mm, respectively. A small hole on the mirrors with perforation diameter of 2 mm to facilitate the passage of the incident beam and the outgoing beam. Through optical simulation, the distance between the mirrors and the angle of incident light were determined to be 138.7 mm and (5.66°, −5.85°), and the incident position coordinate was set to 2.42 mm and 16.8 mm. At last, the multi-pass cell achieved 212 times excitation of the incident light. The schematic diagram and optical path of multi-pass cell are presented in Fig. 2(a) and (b), respectively. The simulation results of incident mirror and exit mirror is plotted in Fig. 2(c) and (d). The surface of concave mirrors was silver-coated to achieve high reflectivity. A visible light with a wavelength of 650 nm was used to verify whether the actual light spot distribution was consistent with the simulation results. Fig. 2(e) and Fig. 2(f) shows the measured spot distribution of the designed multi-pass cell.

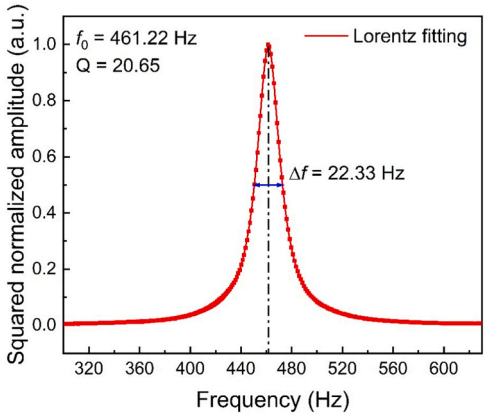

Fig. 4. Frequency response of DHPAC.

3. Experimental setup

Fig. 3 depicts the schematic diagram of a C_2H_2-PAS gas sensor based on DHPAC with a dense spot pattern. In accordance with the HITRAN database, C_2H_2 exhibits a strong absorption peak within the near infrared at 1530.37 nm. Consequently, a diode laser emitting at 1530.3 nm with output power 20 mW was chosen as the excitation light. An erbium-doped fiber amplifier (EDFA) was employed to amplify the optical power of the excitation light. Subsequently, a collimator was utilized to collimate the laser amplified by the EDFA. The transmittance of optical fiber-coupled collimator was 99.75 %. After that, the incident light passes through the entrance hole at a certain angle to complete multiple reflections. In this process, the designed DHPAC was suspended on the multi-pass cell, and one cavity of DHPAC was installed coaxially with the multi-pass cell. The antireflection coated quartz windows with a thickness of 4 mm were used to reduce window losses. The transmittance of the window was 99.8 %. To generate various concentrations of C_2H_2 gas, a bottle of 400 ppm C_2H_2 standard gas was diluted by a bottle of pure nitrogen (N_2), and two mass flow controllers were used to control the flow rate. Two microphones were placed at the strongest point of the acoustic field to obtain the highest photoacoustic signal. Wavelength modulation spectroscopy (WMS) and second harmonic ($2f$) detection were utilized to investigation of the PAS gas sensor. The differential operation of the two microphones was conducted by a differential amplifier. The produced signal was then conveyed into a lock-in amplifier to extract the gas concentration information.

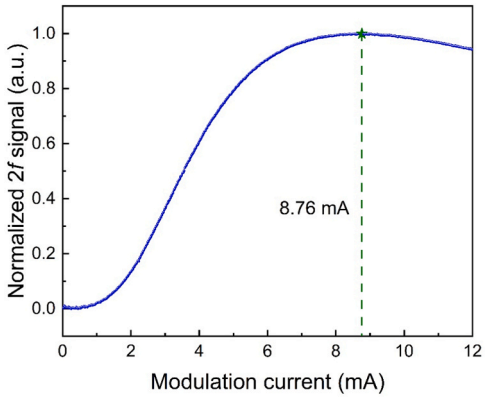

Fig. 5. Modulation current of C_2H_2-PAS sensor based on DHPAC with dense spot pattern.

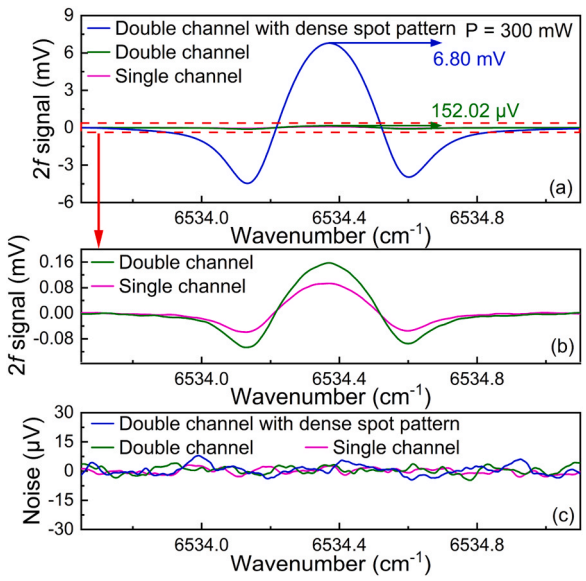

Fig. 6. (a) 2*f* signals of C_2H_2-PAS sensor for single channel, double channel and double channel with dense spot pattern. (b) the enlarged view of 2*f* signals of C_2H_2-PAS sensor for single channel, double channel. (c) The noise of C_2H_2-PAS sensor for single channel, double channel and double channel with dense spot pattern, respectively.

4. Result and discussion

The modulation frequency plays a pivotal role in determining the amplitude of the photoacoustic signal, for the resonant PAS gas sensor system, which must be carefully chosen to match the resonant frequency of the photoacoustic cell. To obtain the strongest photoacoustic signal, the frequency curve of DHPAC was scanned, and the results are represented in Fig. 4. According to the measured results, the resonant frequency of DHPAC could be obtained as 461.22 Hz. Due to the influence of processing errors, the actual resonant frequency of the designed DHPAC deviates from the simulation results. The bandwidth of DHPAC was determined as 22.33 Hz. Therefore, the Q value of the designed DHPAC could be calculated as 20.65.

To ensure the acquisition of the strongest 2*f* signal, it is imperative to optimize modulation current within the PAS system. Fig. 5 illustrates the modulation current profile of the C_2H_2 PAS gas sensor. It can be seen from the scanning results that as the modulation current increases, the photoacoustic signal first increases and then decreases. When the modulation current was set to 8.76 mA, the photoacoustic signal reached its maximum value.

The designed DHPAC with dense spot pattern can achieve 212 times excitation of incident light. However, as the incident light continues to be reflected, the optical power will attenuate exponentially, and the output optical power of the laser is only 20 mW. Therefore, an EDFA was employed to amplify the output optical power of the laser. A bottle of 400 ppm C_2H_2 standard gas was filled into the DHPAC. 2*f* signals of C_2H_2-PAS sensor for single-channel, double channel and double channel with dense spot pattern were obtained when the power level was set to 300 mW, and the obtained are presented in Fig. 6(a) and (b). The peak values of 2*f* signal for single channel, double channel and double channel with dense spot pattern were 90 μV, 152.02 μV and 6.80 mV, respectively. The differential characteristics of DHPAC was verified according to experimental results. Meanwhile, it could be seen that the photoacoustic signal double channel with dense spot pattern had a 44.73 times improvement compared to the double channel without dense spot pattern. The noise obtained by sweeping 2*f* with pure N_2 under different conditions is depicted in Fig. 6(c). The standard deviation of noise for single channel, double channel and double channel with dense spot pattern were 1.39 μV, 2.29 μV and 2.54 μV, respectively.

In order to further enhance the performance of C_2H_2-PAS sensor, the output optical power was increased from 300 mW to 700 mW. Fig. 7 displays the waveforms and peak values of the 2*f* signal from the C_2H_2-PAS sensor under different output optical powers. Concurrently, there is a notable linear relationship between the 2*f* signal peak values and output optical power.

Different concentrations of C_2H_2 were measured to assess the concentration linearity of the C_2H_2-PAS sensor. The output optical power was set to 700 mW. Fig. 8 presents the measured results under different concentration. The R-squared of 0.99988 was achieved, which indicated an exceptionally high degree of linearity between the 2*f* signal peak values and C_2H_2 concentration. The 2*f* signal of each concentration was measured multiple times, and the repeatability fluctuation did not exceed 1 %, indicating that the system has a good repeatability.

For the purpose of evaluating the long-term stability of the designed C_2H_2-PAS sensor, a bottle of pure N_2 was fed to the DHPAC for 2.5 hours. The long-term stability is reflected by the Allan deviation, which is displayed in Fig. 9. The minimum detection limit (MDL) of the designed C_2H_2-PAS sensor can be improved to 5 ppb when the average time is 200 s. The normalized noise equivalent absorption (NNEA) of C_2H_2-PAS sensor based on DHPAC with dense spot pattern was calculated as 6.48×10^{-9} $cm^{-1}W/Hz^{1/2}$.

A comparison of PAS systems for trace C_2H_2 detection based on near infrared laser source is shown in Table 1. According to Table 1, the performance of the designed C_2H_2-PAS sensor has better MDL than the previously reported sensor system.

5. Conclusion

In conclusion, a high-sensitivity C_2H_2-PAS sensor based on DHPAC

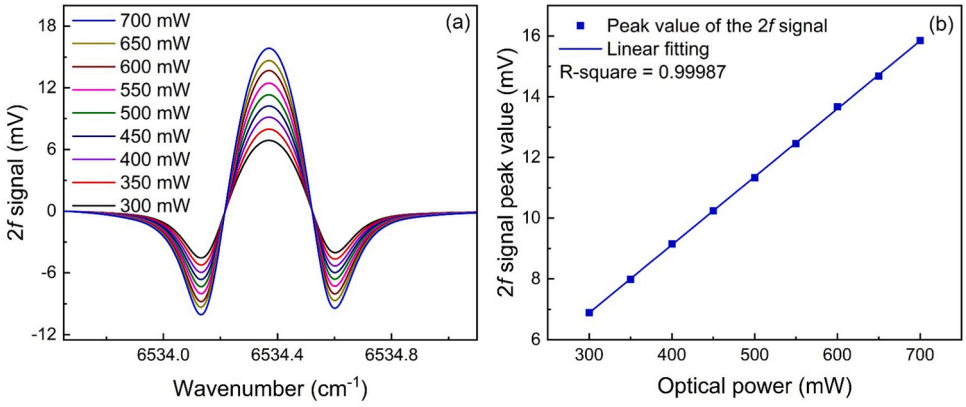

Fig. 7. (a) 2*f* signals of C_2H_2-PAS sensor at different output optical power. (b) 2*f* signal peak values of C_2H_2-PAS sensor as a function of output optical power.

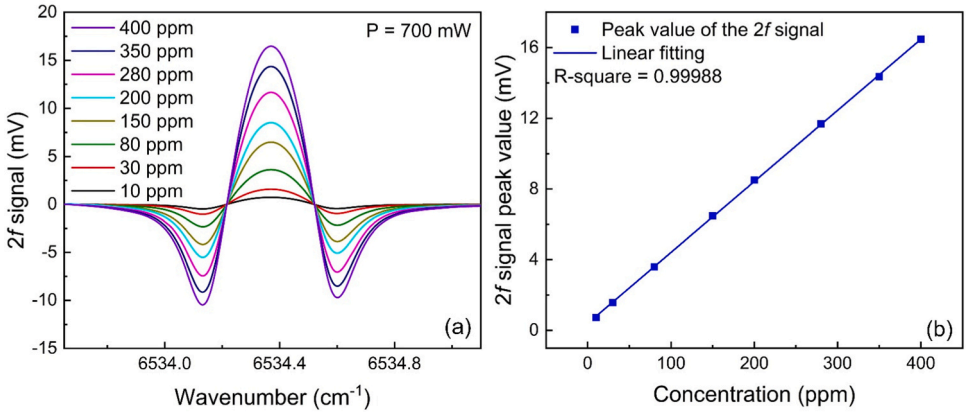

Fig. 8. (a) 2*f* signals of C_2H_2-PAS sensor at different concentration. (b) 2*f* signal peak values of C_2H_2-PAS sensor as a function of C_2H_2 concentration.

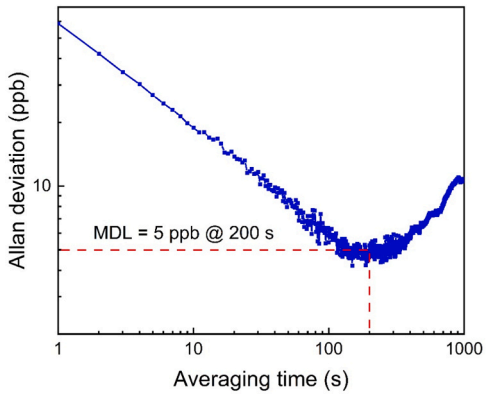

Fig. 9. Allan deviation of C_2H_2-PAS sensor based on DHPAC with dense spot pattern.

Table 1
Comparison of the designed C_2H_2-PAS sensor and previously reported systems.

Ref	Wavelength (nm)	MDL	NNEA ($cm^{-1}W/Hz^{1/2}$)
[49]	1531.588 nm	79.6 ppb	1.4×10^{-9}
[53]	1532.83 nm	12.2 ppb	3.3×10^{-9}
This paper	1530.37 nm	5 ppb	6.48×10^{-9}

with dense spot pattern is presented in this paper for the first time. Based on the finite element analysis method, the sound field distribution and frequency response of DHPAC were calculated. For achieving multiple excitations, a multi-pass cell with dense spot pattern of 212 times excitation of incident laser was designed. The incident light passed through the entrance hole at a certain angle to realize multiple reflections. In this process, the designed DHPAC was suspended on the multi-pass cell, and one cavity of DHPAC was installed coaxially with the multi-pass cell. A diode laser emitting at 1530.3 nm with an output power 20 mW was chosen as the seed laser. An EDFA was employed to amplify the output optical power of the seed laser to achieve strong excitation. According to experimental results, the differential characteristics of DHPAC was realized. The photoacoustic signal amplitude of double channel with dense spot pattern had a 44.73 times improvement compared to the double channel without dense spot pattern. The minimum detection limit (MDL) of the designed C_2H_2-PAS sensor can be improved to 5 ppb when the average time is 200 s.

CRediT authorship contribution statement

Yufei Ma: Writing – review & editing, Supervision, Project administration, Conceptualization. **Shunda Qiao:** Data curation. **Yahui Liu:** Methodology. **Chu Zhang:** Writing – original draft, Investigation. **Ying He:** Methodology.

Declaration of Competing Interest

The authors declare that they have no known competing financial interests or personal relationships that could have appeared to influence the work reported in this paper.

Data Availability

Data will be made available on request.

Acknowledgments

We are grateful for financial supports from the National Natural Science Foundation of China (Grant No. 62335006, 62022032, 62275065, and 61875047), Key Laboratory of Opto-Electronic Information Acquisition and Manipulation (Anhui University), Ministry of Education (Grant No. OEIAM202202), Fundamental Research Funds for the Central Universities (Grant No. HIT.OCEF.2023011).

References

[1] L.X. Liu, H.T. Huan, W. Li, A. Mandelis, Y.F. Wang, L. Zhang, X.S. Zhang, X.K. Yin, Y.X. Wu, X.P. Shao, Highly sensitive broadband differential infrared photoacoustic spectroscopy with wavelet denoising algorithm for trace gas detection, Photoacoustics 21 (2021) 100228.
[2] Y.H. Liu, S.D. Qiao, C. Fang, Y. He, H.Y. Sun, J. Liu, Y.F. Ma, A highly sensitive LITES sensor based on a multi-pass cell with dense spot pattern and a novel quartz tuning fork with low frequency, Opto-Electron. Adv. 7 (2024) 230230.
[3] A. Sampaolo, P. Patimisco, M. Giglio, A. Zifarelli, H.P. Wu, L. Dong, V. Spagnolo, Quartz-enhanced photoacoustic spectroscopy for multi-gas detection: a review, Anal. Chim. Acta 1202 (2022) 338894.
[4] J. Rouxel, J.G. Coutard, S. Gidon, O. Lartigue, S. Nicoletti, B. Parvitte, R. Vallon, V. Zéninari, A. Glière, Miniaturized differential Helmholtz resonators for photoacoustic trace gas detection, Sens. Actuator B-Chem. 236 (2016) 1104–1110.
[5] W.P. Chen, S.D. Qiao, Y. He, J. Zhu, K. Wang, L. Qi, S. Zhou, L.M. Xiao, Y. Ma, Mid-infrared all-fiber light-induced thermoelastic spectroscopy sensor based on hollow-core anti-resonant fiber, Photoacoustics 36 (2024) 100594.
[6] H.Y. Sun, Y. He, S.D. Qiao, Y.H. Liu, Y.F. Ma, Highly sensitive and real-simultaneous CH_4/C_2H_2 dual-gas LITES sensor based on Lissajous pattern multi-pass cell, Opto-Electron. Sci. 3 (2024) 240013.
[7] Y.F. Ma, T.T. Liang, S.D. Qiao, X.N. Liu, Z.T. Lang, Highly sensitive and fast hydrogen detection based on light-induced thermoelastic spectroscopy, Ultra Sci. 3 (2023) 0024.
[8] H. Ge, W.P. Kong, R. Wang, G. Zhao, W.G. Ma, W.G. Chen, F. Wan, Simple technique of coupling a diode laser into a linear power buildup cavity for Raman gas sensing, Opt. Lett. 48 (8) (2023) 2186–2189.
[9] F. Wan, R. Wang, H. Ge, W.P. Kong, H.C. Sun, H.Y. Wu, G. Zhao, W.G. Ma, W. G. Chen, Optical feedback frequency locking: impact of directly reflected field and responding strategies, Opt. Express 32 (7) (2024) 12428–12437.

[10] J.F. Hou, X.N. Liu, Y.H. Liu, Y. He, W.J. Zhao, Y.F. Ma, Highly sensitive CO_2-LITES sensor based on a self-designed low-frequency quartz tuning fork and fiber-coupled MPC, Chin. Opt. Lett. 22 (7) (2024) 073001.
[11] Z.H. Zheng, S.K. Zhu, Y. Chen, H.Y. Chen, J.H. Chen, Towards integrated mode-division demultiplexing spectrometer by deep learning, Opto-Electron. Sci. 1 (11) (2022) 220012.
[12] A. Zifarelli R. De Palo P. Patimisco M. Giglio A. Sampaolo S. Blaser J. Butet O. Landry A. Müller V. Spagnolo Multi-gas quartz-enhanced photoacoustic sensor for environmental monitoring exploiting a Vernier effect-based qu antum cascade laser Photoacoustics 28 2022 100401.
[13] X.Y. Wang, X.K. Qiu, M.L. Liu, F. Liu, M.M. Li, L.P. Xue, B.H. Chen, M.R. Zhang, P. Xie, Flat soliton microcomb source, Opto-Electron. Sci. 2 (12) (2023) 230024.
[14] T.T. Liang, S.D. Qiao, Y.J. Chen, Y. He, Y.F. Ma, High-sensitivity methane detection based on QEPAS and H-QEPAS technologies combined with a self-designed 8.7 kHz quartz tuning fork, Photoacoustics 36 (2024) 100592.
[15] J.M. Le, Y.D. Su, C.S. Tian, A.H. Kung, Y.R. Shen, A novel scheme for ultrashort terahertz pulse generation over a gapless wide spectral range: Raman-resonance-enhanced four-wave mixing, Light Sci. Appl. 12 (1) (2023) 34.
[16] Z.T. Lang, S.D. Qiao, T.T. Liang, Y. He, L. Qi, Y.F. Ma, Dual-frequency modulated heterodyne quartz-enhanced photoacoustic spectroscopy, Opt. Express 32 (1) (2024) 379–386.
[17] B.X. Xu, X.Y. Fan, S. Wang, Z.Y. He, Sub-femtometer-resolution absolute spectroscopy with sweeping electro-optic combs, Opto-Electron. Adv. 5 (2022) 210023.
[18] Y.Q. Wang, J.H. Zhang, Y.C. Zheng, Y.R. Xu, J.Q. Xu, J. Jiao, Y. Su, H.F. Lü, K. Liang, Brillouin scattering spectrum for liquid detection and applications in oceanography, Opto-Electron. Adv. 6 (1) (2023) 220016.
[19] L. Zhang, M. Zhang, T.N. Chen, D.J. Liu, S.H. Hong, D.X. Dai, Ultrahigh-resolution on-chip spectrometer with silicon photonic resonators, Opto-Electron. Adv. 5 (7) (2022) 210100.
[20] M.R. Shao, C. Ji, J.B. Tan, B.Q. Du, X.F. Zhao, J. Yu, B.Y. Man, K.C. Xu, C. Zhang, Z. Li, Ferroelectrically modulate the Fermi level of graphene oxide to enhance SERS response, Opto-Electron. Adv. 6 (11) (2023) 230094.
[21] C. Zhang, Y. He, S.D. Qiao, Y.F. Ma, Differential integrating sphere-based photoacoustic spectroscopy gas sensing, Opt. Lett. 48 (19) (2023) 5089–5092.
[22] Y. Huang, T. Zhang, G.X. Wang, Y.X. Xing, S.L. He, Wavelength-modulated photoacoustic spectroscopy sensor for multi-gas measurement of acetone, methane, and water vapor based on a differential acoustic resonator, Appl. Phys. Lett. 122 (11) (2023) 111105.
[23] S.D. Qiao, Y. He, H.Y. Sun, P. Patimisco, A. Sampaolo, V. Spagnolo, Y.F. Ma, Ultra-highly sensitive dual gases detection based on photoacoustic spectroscopy by exploiting a long-wave, high-power, wide-tunable, single-longitudinal-mode solid-state laser, Light Sci. Appl. 13 (2024) 100.
[24] C. Fang, T.T. Liang, S.D. Qiao, Y. He, Z.C. Shen, Y.F. Ma, Quartz-enhanced photoacoustic spectroscopy sensing using trapezoidal-and round-head quartz tuning forks, Opt. Lett. 49 (3) (2024) 770–773.
[25] Z.T. Lang, S.D. Qiao, Y.F. Ma, Fabry–Perot-based phase demodulation of heterodyne light-induced thermoelastic spectroscopy, Light Adv. Manuf. 4 (2023) 23.
[26] W.P. Chen, S.D. Qiao, Z.X. Zhao, S.F. Gao, Y.Y. Wang, Y.F. Ma, Sensitive carbon monoxide detection based on laser absorption spectroscopy with hollow-core antiresonant fiber, Microw. Opt. Technol. Lett. 66 (1) (2024) e33780.
[27] W.P. Chen, S.D. Qiao, Y. He, J. Zhu, K. Wang, L.M. Xiao, Y.F. Ma, Quasi-distributed quartz enhanced photoacoustic spectroscopy sensing based on hollow waveguide micropores, Opt. Lett. 49 (10) (2024) 2765–2768.
[28] G.J. Wu, X. Wu, Z.F. Gong, J.W. Xing, Y.M. Fan, J.S. Ma, W. Peng, Q.X. Yu, L. Mei, Highly sensitive trace gas detection based on a miniaturized 3D-printed Y-type resonant photoacoustic cell, Opt. Express 31 (21) (2023) 34213–34223.
[29] Q. He, W.R. Zhu, H.F. Lv, X.Y. Wen, Z.X. Zheng, J.F. Wang, M. Li, Multi-MEMS-microphone schemes in a miniature photoacoustic cell for acetylene trace gas measurement, Appl. Opt. 62 (6) (2023) 1647–1653.
[30] C. Zhang, S.D. Qiao, Y. He, Y.F. Ma, Trace gas sensor based on a multi-pass-retro-reflection-enhanced differential Helmholtz photoacoustic cell and a power amplified diode laser, Opt. Express 32 (1) (2024) 848–856.
[31] J.L. Zhang, Z.Q. Meng, J. Xiang, W. Li, L. Xia, W.P. Guo, M. Xia, K.C. Yang, A design methodology of miniature photoacoustic cell based on beam energy distribution and acoustic resonator coupling, Sens. Actuator B-Chem. 410 (2024) 135679.
[32] L. Zhang, L.X. Liu, X.S. Zhang, X.K. Yin, H.T. Huan, H.Y. Liu, X.M. Zhao, Y.F. Ma, X. P. Shao, T-type cell mediated photoacoustic spectroscopy for simultaneous detection of multi-component gases based on triple resonance modality, Photoacoustics 31 (2023) 100492.
[33] Q. Huang, Y. Wei, J.S. Li, Simultaneous detection of multiple gases using multi-resonance photoacoustic spectroscopy, Sens. Actuator B-Chem. 369 (2022) 132234.
[34] S. Alahmari, X.W. Kang, M. Hippler, Diode laser photoacoustic spectroscopy of CO_2, H_2S and O_2 in a differential Helmholtz resonator for trace gas analysis in the biosciences and petrochemistry, Anal. Bioanal. Chem. 411 (2019) 3777–3787.
[35] K. Chen, N. Wang, M. Guo, X.Y. Zhao, H.C. Qi, C.X. Li, G.Y. Zhang, L. Xu, Detection of SF_6 gas decomposition component H2S based on fiber-optic photoacoustic sensing, Sens. Actuator B-Chem. 378 (2023) 133174.
[36] Z.F. Gong, T.L. Gao, L. Mei, K. Chen, Y.W. Chen, B. Zhang, W. Peng, Q.X. Yu, Ppb-level detection of methane based on an optimized T-type photoacoustic cell and a NIR diode laser, Photoacoustics 21 (2021) 100216.
[37] Y. Wei, Q. Huang, J.S. Li, Dual-gas detection based on high-performance spherical photoacoustic cells, Sens. Actuator A-Phys. 360 (2023) 114542.
[38] Q.Y. Ma, L. Li, Z.J. Gao, S. Tian, J.X. Yu, X.C. Du, Y.Y. Qiao, C.X. Shan, Near-infrared sensitive differential Helmholtz-based hydrogen sulfide photoacoustic sensors, Opt. Express 31 (9) (2023) 14851–14861.
[39] X.K. Yin, L. Dong, H.P. Wu, H.D. Zheng, W.G. Ma, L. Zhang, W.B. Yin, S.T. Jia, F. K. Tittel, Sub-ppb nitrogen dioxide detection with a large linear dynamic range by use of a differential photoacoustic cell and a 3.5 W blue multimode diode laser, Sens. Actuator B-Chem. 247 (2017) 329–335.
[40] Z.G. Li, J.X. Liu, G.S. Si, Z.Q. Ning, Y.H. Fang, Active noise reduction for a differential Helmholtz photoacoustic sensor excited by an intensity-modulated light source, Opt. Express 31 (2) (2023) 1154–1166.
[41] H.P. Xiao, J.B. Zhao, C.T. Sima, P. Lu, Y.H. Long, Y. Ai, W.J. Zhang, Y.F. Pan, J. S. Zhang, D.M. Liu, Ultra-sensitive ppb-level methane detection based on NIR all-optical photoacoustic spectroscopy by using differential fiber-optic microphones with gold-chromium composite nanomembrane, Photoacoustics 26 (2022) 100353.
[42] F.P. Wang, L.Y. Fu, J.H. Wu, J.G. Zhang, Q. Wang, A compact photoacoustic detector for trace acetylene based on 3D-printed differential Helmholtz resonators, IEEE Sens. J. 23 (22) (2023) 27207–27214.
[43] Y.Y. Qiao, L.P. Tang, Y. Gao, F.T. Han, C.G. Liu, L. Li, C.X. Shan, Sensitivity enhanced NIR photoacoustic CO detection with SF_6 promoting vibrational to translational relaxation process, Photoacoustics 25 (2022) 100334.
[44] X.K. Yin, M. Gao, R.Q. Miao, L. Zhang, X.S. Zhang, L.X. Liu, X.P. Shao, F.K. Tittel, Near-infrared laser photoacoustic gas sensor for simultaneous detection of CO and H_2S, Opt. Express 29 (21) (2021) 34258–34268.
[45] H.D. Zheng, Y.H. Liu, H.Y. Lin, R.F. Kan, P. Patimisco, A. Sampaolo, M. Giglio, W. G. Zhu, J.H. Yu, F.K. Tittel, Sub-ppb-level CH_4 detection by exploiting a low-noise differential photoacoustic resonator with a room-temperature interband cascade laser, Opt. Express 28 (13) (2020) 19446–19456.
[46] C.X. Li, K. Chen, J.K. Zhao, H.C. Qi, X.Y. Zhao, F.X. Ma, X. Han, M. Guo, R. An, High-sensitivity dynamic analysis of dissolved gas in oil based on differential photoacoustic cell, Opt. Lasers Eng. 161 (2023) 107394.
[47] Z.G. Li, J.X. Liu, G.S. Si, Z.Q. Ning, Y.H. Fang, Design of a high-sensitivity differential Helmholtz photoacoustic cell and its application in methane detection, Opt. Express 30 (16) (2022) 28984–28996.
[48] X.Y. Zhao, F.X. Ma, H. Wang, H.C. Qi, C.X. Li, M. Guo, K. Chen, Fiber-optic photoacoustic CO sensor for gas insulation equipment monitoring based on cantilever differential lock-in amplification and optical excitation enhancement, Anal. Chem. 96 (2024) 5298–5306.
[49] B. Zhang, K. Chen, Y.W. Chen, B.L. Yang, M. Guo, H. Deng, F.X. Ma, F. Zhu, Z. F. Gong, W. Peng, Q.X. Yu, High-sensitivity photoacoustic gas detector by employing multi-pass cell and fiber-optic microphone, Opt. Express 28 (5) (2020) 6618–6630.
[50] Y.F. Li, G.Y. Guan, Y. Lu, X.T. Liu, S. Yang, C.T. Zheng, F. Song, Y. Zhang, Y. D. Wang, F.K. Tittel, Highly sensitive near-infrared gas sensor system using a novel H-type resonance-enhanced multi-pass photoacoustic cell, Measurement 220 (2023) 113380.
[51] X.Y. Zhao, K. Chen, D.Y. Cui, M. Guo, C.X. Li, H.C. Qi, G.Y. Zhang, Z.F. Gong, Z. Zhou, W. Peng, Ultra-high sensitive photoacoustic gas detector based on differential multi-pass cell, Sens. Actuator B-Chem. 368 (2022) 132124.
[52] R.Y. Cui, L. Dong, H.P. Wu, S.Z. Li, X.K. Yin, L. Zhang, W.G. Ma, W.B. Yin, F. K. Tittel, Calculation model of dense spot pattern multi-pass cells based on a spherical mirror aberration, Opt. Lett. 44 (5) (2019) 1108–1111.
[53] M. Zhang, B. Zhang, K. Chen, M. Guo, S. Liu, Y.W. Chen, Z.F. Gong, Q.X. Yu, Z. Q. Chen, M.F. Liao, Miniaturized multi-pass cell based photoacoustic gas sensor for parts-per-billion level acetylene detection, Sens. Actuator A-Phys. 308 (2020) 112013.

Chu Zhang received her B.S. degree in Qingdao University of Technology, China, in 2019. Then, she obtained a master's degree in control engineering from Northeastern University. She is now pursuing a PhD degree of physical electronics from Harbin Institute of Technology. Her research interest is photoacoustic cell design and photoacoustic spectroscopy.

Ying He obtained his master and doctorate degrees in physical electronics from Harbin Institute of Technology in 2017 and 2022, respectively. Currently, he is an associate professor at the Harbin Institute of Technology, China. His research interests including trace gas sensing based on QEPAS, LITES and other laser spectroscopy.

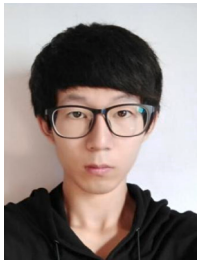

Shunda Qiao received his B.S. degree in electronic science and technology from Yanshan university, China, in 2018. In 2020, he received his M.S. degree and began to pursue a PhD degree of physical electronics from Harbin Institute of Technology. His research interests include photoacoustic spectroscopy and its applications.

Yahui Liu received his B.S. degree in electronic science and technology from Harbin Institute of Technology, China, in 2022. In the same year he pursued a master's degree in physical electronics from Harbin Institute of Technology. His research interest is focused on the design of multi-pass cell and its related sensor performance.

Yufei Ma received his PhD degree in physical electronics from Harbin Institute of Technology, China, in 2013. From September 2010 to September 2011, he spent as a visiting scholar at Rice University, USA. Currently, he is a professor at Harbin Institute of Technology, China. He is the winner of National Outstanding Youth Science Fund. His research interests include optical sensors, trace gas detection, laser spectroscopy, solid-state laser and optoelectronics. He has published more than 200 publications and given more than 30 invited presentations at international conferences. He serves as area editor for Elsevier *Photoacoustics* and Wiley *Microwave and Optical Technology Letters*, and associate editor for Optica *Optics Express*, SPIE *Optical Engineering* and *Frontiers in Physics*. He also serves as topical editor for CLP *Chinese Optics Letters* and editorial board member for MDPI *Sensors* and *Applied Sciences*.